PERGAMON

International Journal of Heat and Mass Transfer 45 (2002) 4589–4598

International Journal of HEAT and MASS TRANSFER

www.elsevier.com/locate/ijhmt

An experimental and theoretical study of the effects of heat conduction through the support fiber on the evaporation of a droplet in a weakly convective flow

Jeng-Renn Yang, Shwin-Chung Wong *

Department of Power Mechanical Engineering, National Tsing Hua University, Hsinchu 300, Taiwan, ROC

Received 29 August 2001; received in revised form 29 April 2002

Abstract

This study investigates the effect of heat conduction through the support fiber on a droplet's evaporation in a weakly convective flow. Experimentally, a droplet of *n*-heptane or *n*-hexadecane with an initial diameter of 700 or 1000 μm was suspended at the tip of a horizontal or vertical quartz fiber (diameter 50, 150, or 300 μm) to evaporate in an upward hot gas flow (at 490 or 750 K). A simple one-dimensional model of transient conduction is formulated in combination with evaporation of the droplet. The calculations agree well with the experiments. In general, heat conduction through the fiber enhances evaporation, with a stronger effect for a lower gas temperature and a thicker fiber. However, the total heat inputs are attenuated when the fiber's diameter is 300 μm. Orientation of the fiber is unimportant. Also, the evaporation rate is enhanced in an oxygen-containing gas flow, due to the additional heating from oxidation around the droplet.

Keywords: Droplet; Droplet evaporation; Droplet combustion; Support fiber

1. Introduction

Most droplet evaporation and combustion experiments have been conducted with the droplet suspended on a support fiber [1–12] to avoid the experimental difficulties for free-falling droplets, such as in obtaining high-resolution droplet images or in maintaining fixed test conditions. These experiments were under flow conditions of either forced convection [1–4] or natural convection [1,4–10]; at atmospheric [1–6,8–12] or elevated pressures [6–9,11]; at normal gravity [1–10] or microgravity [7,8,11]. The fiber orientation was either horizontal [8,11] or vertical [1–4,6,7,10,12]. The fiber materials included quartz [6,8,9,11,12], glass [1,4,5,7], or metals [2,5,10].

The potential influences of the support fiber on the evaporation rate have been pointed out early. Langstroth et al. [5] compared the evaporation rates for different support fibers. They suspended the droplet (diameter of 1000–2000 μm) in still air from the tip of a glass fiber (diameter of 100 μm), a thermocouple (wire diameter of 80 μm), or a special thermocouple arrangement which was designed to conduct heat more rapidly to the droplet. The air temperature ranged from 283 to 313 K. They found that the droplet evaporation rate with the specially arranged thermocouple was larger than for the regular thermocouple. The droplet suspended from the glass fiber resulted in the smallest evaporation rate. In their temperature range, these variations grew with increasing air temperature.

Kadota and Hiroyasu [13] analyzed the effects of heat conduction through the fiber and liquid-phase radiative absorption on droplet evaporation in a simplified manner. The heat conduction through the fiber was evaluated with a simple one-dimensional steady-state analysis; the

* Corresponding author. Tel.: +886-3-571-5131; fax: +886-3-572-2840.

E-mail address: scwong@pme.nthu.edu.tw (S.-C. Wong).

0017-9310/02/$ - see front matter
PII: S0017-9310(02)00164-3

Nomenclature

c_p	constant-pressure specific heat
d	diameter
D	binary mass diffusivity
Gr	Grashof number
k	thermal conductivity
L	latent heat of evaporation
m	total mass of droplet
$-\dot{m}$	droplet evaporation rate
Nu	Nusselt number
Pe	Peclet number, defined as $RePr_\ell$
$\dot{q}$	rate of heat transfer per unit volume
$\dot{Q}$	heat transfer rate
$R(t)$	droplet radius
Re_d	droplet Reynolds number ($U_\infty d_0/\nu_\infty$)
r	spatial coordinate
Sh	Sherwood number
T	temperature
t	time
U	velocity
X_{O_2}	mole fraction of oxygen

Greek symbols

α	thermal diffusivity
χ	effective conductivity parameter
ξ	dimensionless coordinate in the liquid phase
ρ	density

Subscripts

F	fuel
f	support fiber
g	gas phase
ℓ	liquid phase
m	mean value
r	the reference condition used in Eqs. (9) and (10)
s	droplet surface
t	total
0	initial
∞	ambient

radiative absorption was assumed to occur on the droplet surface, adopting an effective surface absorptance whose value appears too small. Although of only qualitative significance, their calculations indicated significant enhancement of the droplet evaporation rate.

In the experiments of Toker and Stricker [10] for droplet evaporation in still air at room temperature, the droplet (diameter of 2000–3000 μm) was suspended from the tip of either a vertical stainless-steel tube (with 350 μm i.d. and 550 μm o.d.) or a thermocouple of 500 μm wire diameter. The evaporation rate for the droplet on the highly conducting steel tube was found higher than that on the thermocouple. The heat influx through the stainless-steel tube and the thermocouple were estimated to be approximately 200% and 50%, respectively, of the heat influx through the droplet surface.

Shih and Megaridis [14] numerically analyzed the effect of fiber conduction on droplet evaporation under forced convection. To allow for axisymmetrical mathematical formulation, the configuration with the fiber parallel to the flow direction was analyzed. In a gas flow of temperature of 1250–1600 K, enhancement of evaporation with the fiber was indicated in their numerical results for a fiber diameter being 1/7 of the initial droplet diameter.

Avedisian and Jackson [12] observed the effect of a support fiber on the soot patterns for droplets burning in a stagnant ambience in microgravity. With a fiber, the shell-like soot aggregate forming inside the flame was found to evolve into a nonsymmetric configuration. This effect is more significant for a thicker fiber. They also observed the nonlinearity in the variation of $(d/d_0)^2$ due to the influence of the fiber.

In our recent calculations of droplet evaporation under microgravity condition at various pressures [15], we have shown that the heat conduction into the droplet through the support fiber and the radiative absorption of the emission from the furnace wall into the liquid phase are responsible for the significant discrepancies between the experimental [11] and theoretical [16,17] evaporation rates. The experiments have been conducted in a hot furnace with the heptane droplets ($d_0 = 600$–800 μm) suspended by a quartz fiber ($d_f = 150$ μm). However, while these theoretical models [16,17] carefully considered the nonideality of gas-phase properties and enthalpy of evaporation at elevated pressures, the additional heat conduction through the fiber and the absorption of the wall emission into the droplet were not included. To analyze the conduction input through the fiber, a simple one-dimensional transient model was proposed [15]. The radiative absorption in the liquid phase was calculated with geometric optics. When these effects are considered, the theoretical time variations of squared droplet diameter are in good agreement with the experimental data [11] for different temperatures and pressures. The effects of radiative absorption and fiber conduction enhance the evaporation rate significantly. At a temperature as low as 470 K, the discrepancies between the theoretical and experimental results are mainly due to the additional fiber conduction, while at a temperature as high as 750 K, the liquid phase radiative absorption becomes mainly responsible for the discrepancies.

In this work, experimental measurements will be presented to manifest the effects of heat transfer through the support fiber on droplet evaporation. These results will also be used to justify the validity of the simplified one-dimensional model of transient heat conduction through the fiber [15]. To minimize the role of thermal radiation, we conducted experiments in an open, weakly convective hot gas flow. Different droplet sizes, fiber diameters and orientations, gas temperatures, and fuel volatilities are tested. Furthermore, detailed knowledge of how and to what extent the heat conduction through the fiber affects the droplet evaporation rate will be provided with the aid of this model.

2. Experimental

Droplet evaporation experiments were conducted in an upward hot laminar gas flow generated by either a flat flame burner ($T_\infty = 750$ K) or an electrical heater ($T_\infty = 490$ K). Droplets of initial diameter of 700 or 1000 μm were suspended at the tip of a quartz fiber. Investigated fiber diameters are 50, 150, and 300 μm. Initial droplet temperature was kept at about 300 K. The fiber tip had been melted into a bead, with diameter of 150, 300, or 400 μm, respectively for the 50, 150, and 300 μm fiber. The support fiber was either horizontal or vertical, respectively perpendicular or parallel to the gas flow. The flat-flame burner was the same as in [18], where a detailed description of it is available. It was fueled with CO, O_2, and N_2, with gas flow rates controlled by rotameters. The hot post-flame gas either was oxygen free or contained oxygen with a mole fraction of 0.21 (measured with an oxygen analyzer). The oxygen-free gas flow was used for evaporation without oxidation reactions, while the oxygen-containing gas flow was used to observe the effect of the additional heating from the oxidation around the droplet on the evaporation rate. A stainless-steel mesh was placed on top of the quartz chimney to reduce the post-flame gas temperature to 750 K. The mesh was loosely knitted so that radiation from it was negligible. The electrical heater, as shown in Fig. 1, provided a low-temperature continuous air flow ($T_\infty =$ 490 K). The alumina beads and the convergent nozzle at the exit of the heater were used to ensure a uniform laminar flow. Good uniformity for the gas temperature was obtained around the test location for a range of several times of the droplet diameter in both the horizontal and vertical directions.

The gas velocity was measured with a laser Doppler anemometer (one component, Aerometrics) seeded with MgO powder. Gas temperatures were measured with uncoated Pt/Pt–10% Rh (S-type) thermocouples with wire diameter of 25 μm and bead diameter of approximately 50 μm. The effect of radiative loss on temperature measurements was neglected, because the effect was estimated assuming the bead as a sphere with a surface emissivity of 0.15 to decrease the temperature readings by less than 2 K. The uncertainty of temperature measurements was estimated to be within ±5 K.

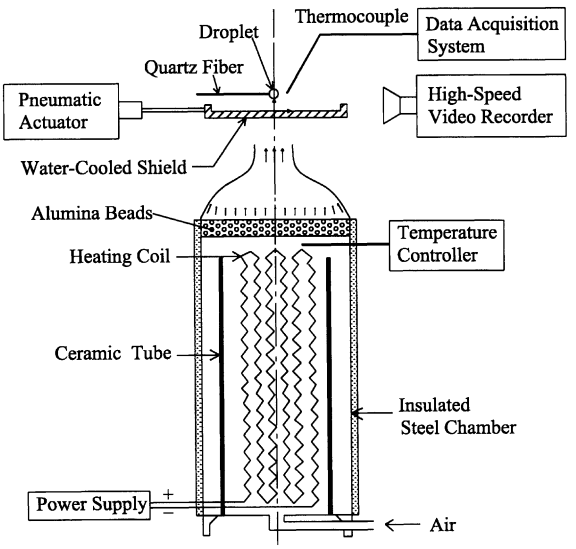

Fig. 1. Electrical heater and test arrangement.

During the test, a suspended droplet was rapidly exposed to the hot gas flow by quickly withdrawing a water-cooled shield, which protected the droplet from the hot gas prior to experiment. After the withdrawal of the shield, a transient period existed before flow conditions became steady, as shown in Fig. 2 for a representative temperature history. To measure the transient temperature response, a butt-welded S-type thermocouple (25 μm wire diameter) was used. The thermocouple response delay to attain 95% of the temperature

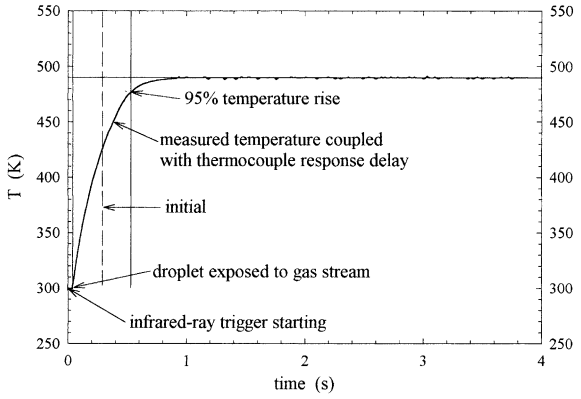

Fig. 2. Gas temperature readings and critical events during the early stage of convective heating.

Table 1
Test conditions

T_∞ (K)	Generator	X_{O_2}	U_∞ (m/s)
490	Electrical heater	0.21	0.7
750	Flat flame burner	0	0.6
750	Flat flame burner	0.21	0.6

rise was calculated to be about 45 ms. Therefore, after subtracting the 45 ms thermocouple response delay, the transient period was about 500 ms, counting from the beginning up to the attainment of 95% of the temperature rise, as shown in Fig. 2 for the $T_\infty = 490$ K case. The transient period for the $T_\infty = 750$ K flow was 450 ms. The reference time for the initiation of a test was selected at the middle of the transient period. In reducing the diameter variation data, this initial reference time was considered as the beginning of the evaporation process. This selection of the initial reference time was somewhat arbitrary and the uncertainty associated with it was roughly of O (100 ms). However, this uncertainty, arising from different initial temperature environments in the experimental and theoretical methods, only influences the time-wise agreement between the experimental and theoretical results. For different runs under the same flow condition, the same initial reference time was used. Therefore, the uncertainties that are relevant to the significance of the differences among experimental measurements are those associated with the consistency of the transient periods in different runs. Such uncertainties, determined by examining the deviations of the initial periods for different runs under the same flow condition, were less than ±20 ms.

The evaporation process was recorded with a high-speed video recorder (NAC, SHV-1000) at a framing rate of 500 fps. The droplet images were then transferred to a personal computer, on which the droplet diameters were measured with the surface boundary determined using an image processing software. The effective diameter was evaluated by approximating the droplets as ellipsoids. The uncertainty of the diameter measurement was within ±15 μm.

The test conditions are summarized in Table 1. The droplet Reynolds numbers ($Re_d = U_\infty d_0/\nu_\infty$) for all our tests ranged from 5 to 17.

3. Theoretical

The physical problem simulated is as follows. A single droplet ($d_0 = 700$ or 1000 μm) suspended at the tip of a horizontal quartz fiber ($d_f = 50$–300 μm) is evaporating in an upward laminar hot gas flow with a uniform temperature T_∞ and a uniform velocity U_∞. The droplet is subjected to heat input through its surface as well as the heat conduction through the fiber. The situation for a vertical fiber (parallel to the flow) is not considered because the temperature and velocity distributions in the wake of the droplet, where the fiber is exposed, are complicated.

3.1. Droplet evaporation model

To simulate the transient droplet evaporation process in a convective flow, we adopt the film theory to account for the heat and mass transfer between the droplet and the ambience, using the semi-empirical relations proposed by Haywood et al. [19]. This approach employs a one-dimensional, spherically symmetric liquid-phase model. The asymmetric effects caused by the presence of the fiber are neglected. Local thermodynamic equilibrium is assumed at the liquid–vapor interface. For the heat transfer analysis in the droplet interior, the effective conductivity model is used. The internal heat transfer is assumed to be unaffected by the presence of the fiber. It is noted that this assumption, as well as the assumption of spherical symmetry, becomes less appropriate for a small (d/d_f) ratio, i.e. a small droplet on a large fiber and during the late lifetime. Since a small (d/d_f) ratio is avoided in most experimental studies (except during the late lifetime), this will not limit the applicability of this model.

In the experiments, the buoyancy induces downward flow opposing the upward hot gas flow. However, the effect of buoyancy is neglected in the model due to the following reasons. First, this effect has been experimentally shown to exhibit slight effect to the droplet evaporation rate at atmospheric pressure. Second, the maximum ratios of (Gr_d/Re_d^2) during the evaporation process of a droplet in the present test conditions range from 0.005 to 0.02. Since these values are much smaller than unity, the buoyancy effect is negligible [20]. Furthermore, the main objective of this study is to investigate the effect of heat conduction through the fiber both experimentally and theoretically. Therefore, neglecting natural convection in the model should be acceptable.

Further assuming that the heat input through the fiber is uniformly distributed to the droplet, the governing equations for the liquid phase are

$$-\dot{m} = \frac{\mathrm{d}m}{\mathrm{d}t} = 4\pi R^2 \left(\frac{\mathrm{d}R}{\mathrm{d}t}\rho_{\ell,\mathrm{m}} + \frac{R}{3}\frac{\mathrm{d}\rho_{\ell,\mathrm{m}}}{\mathrm{d}t} \right) \tag{1}$$

and

$$\rho_\ell c_{p,\ell}\frac{\partial T_\ell}{\partial t} = \frac{\chi k_\ell}{r^2}\frac{\partial}{\partial r}\left(r^2 \frac{\partial T_\ell}{\partial r} \right) + \dot{q}_f, \tag{2}$$

where $\dot{q}_f$ is the heat input through the fiber, which will be discussed later.

The initial and boundary conditions are

$$T_\ell(r,0) = T_0, \tag{3}$$

$$\dot{Q}_s = \dot{m}L + 4\pi r_s^2 \chi k_\ell \left.\frac{\partial T_\ell}{\partial r}\right|_{r=r_s}, \tag{4}$$

and

$$\left.\frac{\partial T_\ell}{\partial r}\right|_{r=0} = 0. \tag{5}$$

The effective conductivity parameter χ has been suggested [21] as

$$\chi = 1.86 + 0.86\tanh[2.245\log_{10}(Pe_\ell/30)], \tag{6}$$

where Pe_ℓ is the liquid's Peclet number, defined as $Re_d Pr_\ell$. The heat and mass transfer rates are estimated by

$$\dot{m} = 2\pi r_s \rho D Sh B_Y \tag{7}$$

and

$$\dot{Q}_s = 2\pi r_s k Nu(T_\infty - T_s). \tag{8}$$

The Nusselt and the Sherwood number are determined by [19]

$$Nu(1+B')^{0.7} = 2 + 0.57 Re_r^{1/2} Pr_r^{1/3} \tag{9}$$

and

$$Sh(1+B_Y)^{0.7} = 2 + 0.87 Re_r^{1/2} Sc_r^{1/3}, \tag{10}$$

where $B' = (c_p(T_\infty - T_s)/L)(1 - \dot{Q}_\ell/\dot{Q}_s)$ and $B_Y = (Y_{F,s} - Y_{F,\infty})/(1 - Y_{F,s})$. The droplet's heating rate was calculated as $\dot{Q}_\ell = \dot{Q}_s - \dot{m}L$. The properties of the gas mixtures used in the semi-empirical relations (Eqs. (9) and (10)) are calculated based on the reference temperature and fuel concentration defined as

$$T_r = \frac{1}{2}T_s + \frac{1}{2}T_\infty, \qquad Y_{F,r} = \frac{1}{2}Y_{F,s} + \frac{1}{2}Y_{F,\infty}.$$

For example, $c_{p,m} = c_{p,F}Y_{F,r} + c_{p,g}(1 - Y_{F,r})$.

3.2. Calculation of fiber conduction input $\dot{Q}_f(t)$

To calculate the conduction input through the fiber, we use a transient one-dimensional model described as follows.

Since the fiber is fine and the Biot numbers are of $O(10^{-2})$, the temperature distribution in the fiber is assumed one dimensional. The conservation of energy can be written as

$$\rho_f c_{p,f} \frac{\partial T_f}{\partial t} = k_f \frac{\partial^2 T_f}{\partial x^2} + \frac{4h_\infty}{d_f}(T_\infty - T_f). \tag{11}$$

In Eq. (11), h_∞, the heat convection coefficient over a horizontal cylinder, is obtained with $h_\infty = Nu_\infty k_\infty/d_f$. For the portion exposed to the gas flow ($x > R$), [22]

$$Nu_{g,\infty} = 0.3 + \frac{0.62 Re_{d_f}^{1/2} Pr^{1/3}}{\left[1 + (0.4/Pr)^{2/3}\right]^{1/4}} \times \left[1 + \left(\frac{Re_{d_f}}{2.82\times 10^5}\right)^{5/8}\right]^{4/5},$$

and for the portion emerged in the droplet ($-R \leqslant x \leqslant R$), $Nu_{\ell,\infty} = 0.36$, as for a limiting stagnant situation [23]. This approximation limits the applicability of this model to a weakly convective flow. For the emerged portion, T_∞ is replaced by $T_\ell(x)$.

The initial condition is : $T_f(0,x) = T_0$, (12)

The boundary condition at $x \to \infty$ is : $\dfrac{\partial T_f}{\partial x} = 0.$ (13)

The other boundary condition at the tip of the fiber, where the droplet is positioned, can be approximated as [15]:

$$\frac{\partial T_f}{\partial x} \approx 0 \text{ at } x = 0. \tag{14}$$

The properties of the fiber are $\rho_f = 2.22$ g/cm^3, $k_f = 3.29\times 10^{-3}$ cal/cm s K, and $c_{p,f} = 0.178$ cal/g [24]. With T_f solved from Eqs. (11)–(14), the conduction input through the fiber can be calculated by

$$\dot{Q}_f = \int_{x=-R}^{x=R} h_{\ell,\infty}(T_\ell(x) - T_f(x))\pi d_f \,\mathrm{d}x$$

and

$$\dot{q}_f = \left(\int_{x=-R}^{x=R} h_{\ell,\infty}(T_\ell(x) - T_f(x))\pi d_f \,\mathrm{d}x\right)/V_{net},$$

where V_{net} is the net volume of the liquid fuel (the fiber volume excluded).

3.3. Thermophysical properties

The density, specific heat, and thermal conductivity of the liquid fuels (*n*-heptane and *n*-hexadecane) are calculated following Daubert and Danner [25]. Calculations of latent heat of evaporation and the saturated vapor pressure also follow Daubert and Danner [25].

Gas-phase thermophysical properties are calculated for the fuel vapor, nitrogen and their mixtures, assuming that the gas mixture consists of nitrogen and fuel vapor. With the ideal-gas assumption, the density of the gas mixture is calculated from the equation of the state with the molecular weight of the mixture. Thermal conductivities follow the modified Eucken method [26] for the fuel vapors and Daubert and Danner [25] for nitrogen. Specific heats of them are obtained from Daubert and Danner [25]. The gas phase binary mass diffusivity D for heptane–nitrogen or hexadecane–nitrogen mixtures is calculated using the Chapman and Enskog theory [26].

3.4. Numerical procedure

To account for the droplet surface regression during evaporation, transformation of the spatial coordinate, r, in the liquid phase is made to fix the surface by changing r to $\xi(r,t)$, where $\xi(r,t) = r/R(t)$, $0 \leqslant \xi(r,t) \leqslant 1$ [15]. The numerical scheme forward in time and central in space is used to discretize the governing equations and boundary conditions. In our numerical experimentation, the time step, Δt, has been carefully chosen to satisfy the stability criterion and the grid size $\Delta\xi = 0.01$ is adequately small for all of our computations. The thermophysical properties are calculated in each time step before the liquid phase governing equations are solved.

4. Results and discussion

In our experiments, droplets tested are of two different sizes (700 and 1000 μm) and two fuels of different volatilities (n-heptane, b.p. = 372 K; n-hexadecane, b.p. = 560 K). Two environment temperatures (490 and 750 K) and two different fiber orientations (cross-flow or parallel-flow) were arranged. For each test condition, five runs were made. The repeatability was good, as will be shown by the two runs presented with open and filled symbols for each condition.

Fig. 3 shows the time variations of squared diameter for n-heptane and n-hexadecane droplets in the 490 K air flow. For all these three test conditions, the agreement between the theoretical and experimental results are excellent, and the effect of the heat conduction through the fiber on the evaporation rate is satisfactorily predicted by our simplified model for various fiber diameters. For this low-temperature condition, the fiber effect is clearly manifested. In general, the droplets shrink faster for a larger fiber, especially during the late period. Also, the evaporation enhancement due to fiber conduction appears at an earlier lifetime for small droplets with $d_0 = 700$ μm, whose volumes are only about 1/3 of those large droplets with $d_0 = 1000$ μm. This is shown in Fig. 3a in that deviation of the evaporation rates appears when $(d/d_0)^2 \sim 0.8$ for $d_0 = 700$ μm, in comparison with $(d/d_0)^2 \sim 0.7$ for $d_0 = 1000$ μm. In general, the fiber conduction effect is stronger for a smaller (d_0/d_f) ratio. For the nonvolatile hexadecane droplets with $d_0 = 700$ μm (Fig. 3b), a considerable portion of the lifetimes are consumed by droplet heating during which no significant shrinking is rendered. In this condition, the evaporation enhancement manifests after $(d/d_0)^2 \sim 0.9$.

Deeper knowledge of the fiber conduction effect can be obtained from the theoretical results illustrated in Fig. 4. For $T_\infty = 490$ K and $d_0 = 700$ μm, the time variations of the total heat input ($\dot{Q}_t$) along with the partial inputs through the droplet surface ($\dot{Q}_s$) and

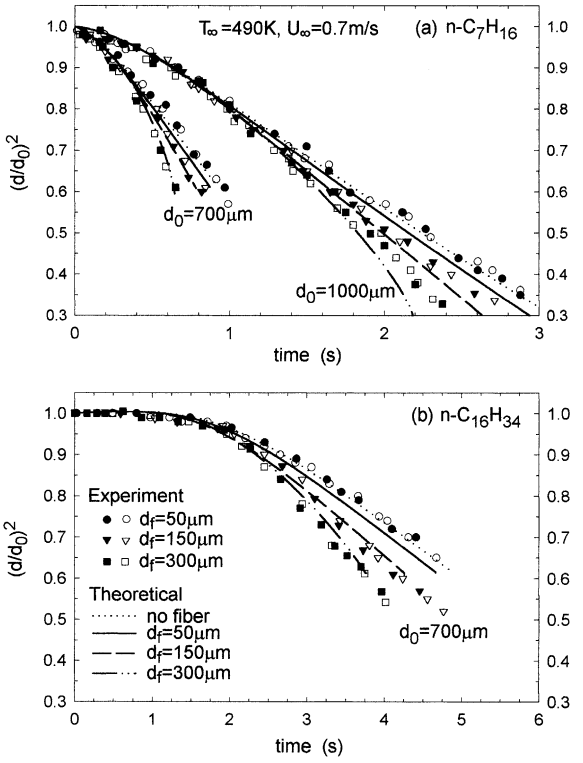

Fig. 3. Theoretical and experimental time variations of normalized squared droplet diameter for different fiber diameters, $T_\infty = 490$ K and $U_\infty = 0.7$ m/s. (a) n-heptane droplets of $d_0 = 750$ and 1000 mm, (b) n-hexadecane droplets of $d_0 = 750$ μm.

through the fiber ($\dot{Q}_f$) are shown for heptane (Fig. 4a) and hexadecane (Fig. 4b) droplets. The time variations of these inputs depend on the temperature differences between the ambient gas, the droplet and the fiber. While the ambient gas conditions are fixed, the droplet temperature is a function of droplet size, fuel volatility and $(\rho c_p)_\ell$; and fiber temperature of fiber size and $(\rho c_p)_f$. Since $(\rho c_p)_\ell \sim (\rho c_p)_f$ in this study and T_∞ and d_0 are fixed in Fig. 4, fuel volatility and fiber size are the important parameters in considering these heat inputs. For the volatile heptane droplets, the droplet lifetime are relatively short that the heat input through the fiber still undergoes a transient state during the early period, especially for the cases with thick fibers. For the finest fiber ($d_f = 50$ μm), $\dot{Q}_f$ becomes steady rapidly. However, the heat input through the droplet surface $\dot{Q}_s$ becomes slightly less than that without a fiber (represented by the $\dot{Q}_t$ curve with no fiber). This is because the additional heat input through the fiber quickens the droplet temperature rise to lessen the temperature difference between the ambient gas and the droplet surface and hence $\dot{Q}_s$. Nevertheless, the total heat input ($\dot{Q}_t = \dot{Q}_s + \dot{Q}_f$) is enhanced with the fiber. The fiber effect is magnified for

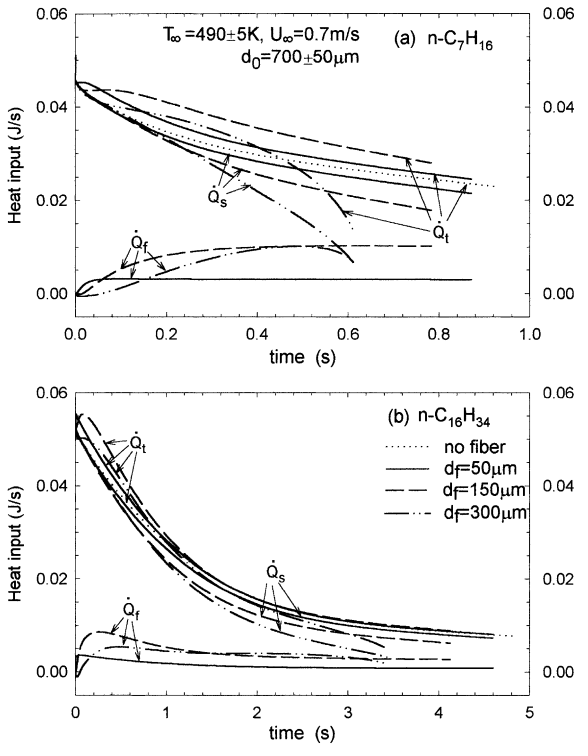

Fig. 4. Calculated time variations of heat transfer rates for different fiber diameters, $T_\infty = 490$ K, $U_\infty = 0.7$ m/s, and $d_0 = 750$ μm. (a) *n*-heptane droplets, (b) *n*-hexadecane droplets. $\dot{Q}_t$—rate of total heat input; $\dot{Q}_s$—rate of heat input through droplet surface; $\dot{Q}_f$—rate of heat input through fiber.

$d_f = 150$ μm, and the total heat input is enlarged significantly. When $d_f = 300$ μm, some interesting behaviors are observed. There exists a short period with negative $\dot{Q}_f$ (heat conduction from the droplet to the fiber), after which $\dot{Q}_f$ slowly increases to a maximum and then decreases. The slow increase of $\dot{Q}_f$ during the early period is because of the long heat-up time needed for this thick fiber. The maximum occurs when the fiber has been heated sufficiently but the droplet temperature is still low. Afterwards, since the fraction of the net liquid volume in the apparent droplet volume is less for a larger d_f (for example, when $d_f = 300$ μm and $d_0 = 700$ μm, the fraction changes from 0.72 to 0.54 for $(d/d_0)^2$ from 1.0 to 0.6), the droplet temperature rises rapidly to reach a higher distribution than for finer fibers. Consequently, $\dot{Q}_f$ decreases with the smaller temperature difference between the fiber and the droplet. In addition, the decrease of the wetted fiber surface area following the droplet shrinkage also contributes to the fast decrease of $\dot{Q}_f$ during the late lifetime. Another consequence of the rapid rise of droplet temperature for large d_f shows in the accelerated dropping of $\dot{Q}_s$ for $d_f = 300$ μm. Among the three fiber diameters, the largest total heat inputs are found for $d_f = 150$ μm. Although the total input for $d_f = 300$ μm is always less than for $d_f = 150$ μm, the evaporation rate for it is larger. This is because the smaller net liquid volume leads to faster droplet temperature rise. Although the theoretical analysis is less reliable for such small (d/d_f) ratios ($d_0 = 700$ μm, $d_f = 300$ μm), as explained earlier, the theoretical predictions still agree with the experiments very well (Fig. 3).

For the nonvolatile hexadecane droplets (Fig. 4b), the transient heat-up periods for the fiber are relatively short in comparison with the droplet lifetime. The time variations of $\dot{Q}_s$, $\dot{Q}_f$ and $\dot{Q}_t$ for different fiber diameters are not as different as for the heptane droplets. During the early stage, $\dot{Q}_t$ for $d_f = 150$ μm is again the largest. But after $t = 1.2$ s, all the $\dot{Q}_t$ curves, except for $d_f = 300$ μm, are hardly distinguishable. As far as $\dot{Q}_f$ is concerned, it rapidly reaches a maximum when the temperature difference between the fiber and the droplet is largest. Afterwards, the droplet temperature gradually approaches a wet-bulb temperature, which is closer to 490 K than for a heptane droplet due to the lower volatility of hexadecane. Therefore, the smaller temperature difference between the fiber and the droplet results in smaller $\dot{Q}_f$.

Experimental and theoretical results in the high-temperature gas flow ($T_\infty = 750$ K) are shown in Fig. 5. Except for the slight differences between the calculations and the experiments for heptane droplet with $d_0 = 1000$ μm, the agreement is again very good. Our model provides accurate predictions for the time variations of $(d/d_0)^2$ for all the three fiber diameters. In contrast to the data for $T_\infty = 490$ K (Fig. 3), it can be seen from both experimental and theoretical results that the effect of heat conduction through the fiber is weaker for this high temperature flow condition. This is explained as follows. When the flow temperature is higher the droplet lifetime is greatly shortened but the transient heat-up period for the fiber becomes longer. Since there is less heat input through the fiber during the heat-up period, its effect on evaporation rate becomes weaker.

It should be pointed out that, according to the theoretical results in Figs. 3 and 5, a support quartz fiber as small as $d_f = 50$ μm can be applied in droplet evaporation experiments to avoid significant effect of the heat input through the fiber.

Different fiber orientations, cross-flow or parallel-flow, have been chosen in different droplet evaporation experiments. For the parallel-flow orientation, theoretical analysis is more difficult [14] in that the fiber is exposed in the wake region where the temperature and velocity fields are complicated. In this work, we have investigated the effect of fiber orientation experimentally. We have observed the differences in the time variation of $(d/d_0)^2$ for different gas temperatures, fiber diameters, and fuels. A representative set of experimental results is shown in Fig. 6 for hexadecane droplets

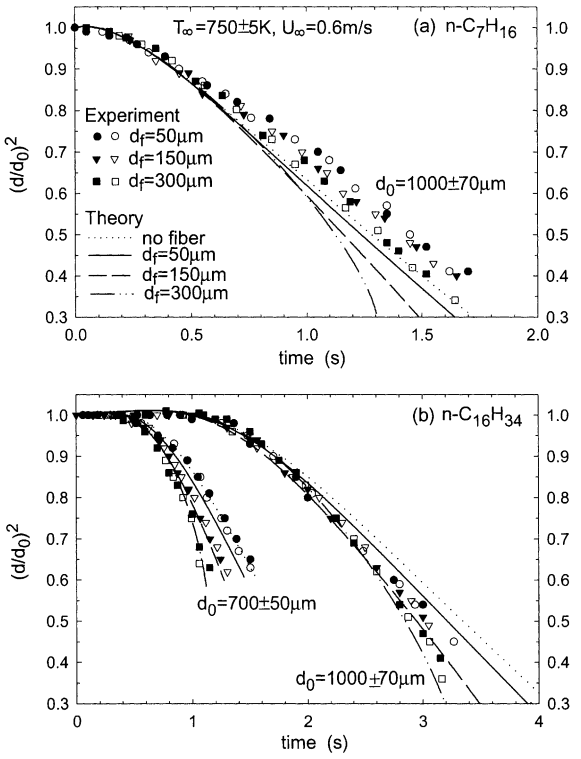

Fig. 5. Theoretical and experimental time variations of normalized squared droplet diameter for different fiber diameters, $T_\infty = 750$ K and $U_\infty = 0.6$ m/s. (a) *n*-heptane droplets of $d_0 = 1000$ μm, (b) *n*-hexadecane droplets of $d_0 = 750$ and 1000 μm.

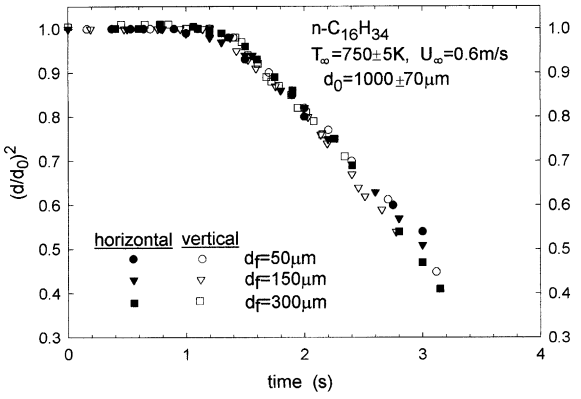

Fig. 6. Effects of fiber orientation on the evaporation for different fiber diameters, $T_\infty = 750$ K, $U_\infty = 0.6$ m/s and $d_0 = 1000$ μm.

($d_0 = 1000$ μm, $T_\infty = 750$ K). While deviations for different fiber diameters can be seen, there is no observable difference between the time variation data for both orientations. This is also true for other test conditions.

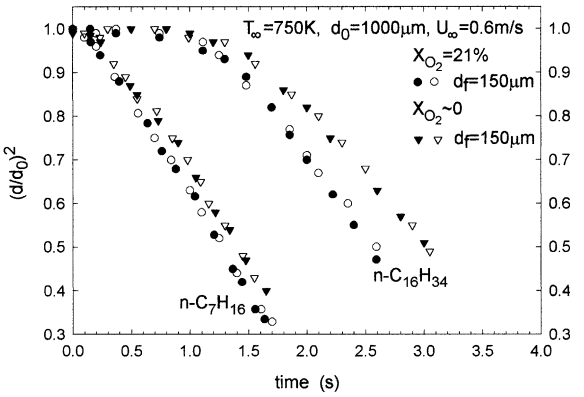

Fig. 7. Effects of oxygen concentration on the evaporation of heptane and hexadecane droplets for different fiber diameters, $T_\infty = 750$ K, $U_\infty = 0.6$ m/s and $d_0 = 1000$ μm.

Fig. 7 illustrates the effect of additional heating from the oxidation around the droplet on the evaporation rate for both heptane and hexadecane droplets ($d_0 = 1000$ μm, $d_f = 150$ μm). Both temperatures of the oxygen-containing ($X_{O_2} = 0.21$) and the oxygen-free gas flow are 750 K. In this temperature range, oxidation of alkane fuels takes place via the low-temperature reaction mechanism [27]. The gas-phase oxidation is shown to enhance the droplet evaporation rate. For hexadecane, this effect appears later but becomes stronger afterwards. This can be explained as follows. While hexadecane and heptane have similar chemical reactivities, their volatilities are very different. During the early heat-up period of the hexadecane droplet, the saturation fuel vapor pressures are still too small to lead to significant oxidation heating. Afterwards, a higher droplet surface temperature can be reached for a hexadecane droplet due to its higher boiling point. The temperature of the adjacent gas mixture is higher so that stronger oxidation prevails to cause a larger evaporation rate for the hexadecane droplet, especially during the late lifetime. Additional heating from the oxidation around the droplet may occur and enhance the evaporation rates for spray droplets in a combustor during their pre-ignition evaporation period. This potential effect has not been reported in the literature.

5. Concluding remarks

This study investigated the effect of support fiber conduction on droplet evaporation in a weakly convective flow. Experimentally, *n*-heptane and *n*-hexadecane droplets with initial diameter of 700 or 1000 μm were suspended at the tip of a horizontal or vertical quartz fiber (diameter of 50, 150, or 300 μm) to evaporate in an upward hot gas flow ($T_\infty = 490$ or 750 K).

For all the tests, the droplet Reynolds number ranged from 5 to 17. Theoretically, a simple one-dimensional model of transient heat conduction was formulated with evaporation of the droplet. The model used the film theory to account for the heat and mass transfer between the droplet and the ambient atmosphere. Excellent agreement was found between the experimental and theoretical results of the droplet diameter history for all the cases tested.

Based on the combined experimental and theoretical investigations, the following conclusions were reached:

1. In a low temperature gas flow ($T_\infty = 490$ K), the fiber conduction enhances the evaporation rate significantly for both heptane and hexadecane droplets. The enhancement intensified with a decrease of the (d_0/d_f) ratio. In a high temperature flow ($T_\infty = 750$ K), the enhancement becomes weaker.
2. Detailed theoretical analysis indicates that while the evaporation rate enhances with increasing fiber diameter d_f, the total heat input $\dot{Q}_t$ does not follow this trend. As d_f increases to 150 μm, $\dot{Q}_t$ does enlarge. But as $d_f = 300$ μm, the droplet temperature rises rapidly so that the heat inputs through the droplet surface and the fiber are attenuated. Consequently, $\dot{Q}_t$ is lowered, especially during the late lifetime.
3. A quartz fiber as small as $d_f = 50$ μm may be adequately applied in droplet evaporation experiments because it has been found to yield insignificant effect of the heat input through the fiber.
4. For a cross-flow and a parallel-flow fiber orientation, there is no observable difference between the experimental results of the time variation of $(d/d_0)^2$.
5. In an oxygen-containing gas flow with sufficiently high temperature (e.g. 750 K), the additional heating from the reactive gas mixture is found to enhance the evaporation rate, with a stronger effect for hexadecane than for heptane droplets.

Acknowledgements

This work was funded by National Science Council, ROC under Contract NSC89-2212-E-007-090.

References

[1] W.E. Ranz, W.R. Marshall, Evaporation from drops: Part 1, Chem. Eng. Prog. 48 (3) (1952) 141–146.
[2] M. Renksizbulut, M.C. Yuen, Numerical study of evaporation in a high-temperature stream, J. Heat Transfer, Trans. ASME 105 (1983) 384–388.
[3] S.-C. Wong, A.-C. Lin, Internal temperature distributions of droplets vaporizing in high-temperature convective flows, J. Fluid Mech. 237 (1992) 671–687.
[4] A. Daïf, M. Bouaziz, A. Chesneau, A.A. Chérif, Comparison of multicomponent fuel droplet vaporization experiments in forced convection with the Sirignano model, Exp. Therm. Fluid Sci. 18 (1999) 282–290.
[5] G.O. Langstroth, C.H.H. Diehl, E.J. Winhold, The evaporation of droplets still air, Canadian J. Res. 28A (1950) 580–595.
[6] H. Hiroyasu, T. Kadota, T. Senda, T. Imamoto, Evaporation of a single droplet at elevated pressures and temperatures, Trans. JSME 40 (339) (1974) 3147–3155.
[7] J.P. Hartfield, P.V. Farrell, Droplet vaporization in a high-pressure gas, J. Heat Transfer, Trans. ASME 115 (1993) 699–706.
[8] R. Ristau, U. Nagel, H. Iglseder, J. Konig, H.J. Rath, H. Nomura, M. Kono, M. Tanage, J. Sato, Theoretical and experimental investigations on droplet evaporation and droplet ignition at high pressures, Microgravity Sci. Tech. VI/4 (1993) 223–228.
[9] C. Chauveau, X. Chesneau, I. Gökalp, High pressure vaporization and burning of methanol droplets in reduced gravity, Adv. Space Res. 16 (7) (1995) 157–160.
[10] G.R. Toker, J. Stricker, Holographic study of suspended vaporizing volatile liquid droplets in still air, Int. J. Heat Mass Transfer 39 (16) (1996) 3475–3482.
[11] H. Nomura, Y. Ujiie, H.J. Rath, J. Sato, M. Kono, Experimental study on high-pressure droplet evaporation using microgravity conditions, in: Proceedings of 26th International Symposium on Combustion, The Combustion Institute, Pittsburgh, PA, 1996, 1267–1273.
[12] C.T. Avedisian, G.S. Jackson, Soot patterns around suspended *n*-heptane droplet flames in a convection-free environment, J. Propulsion Power 16 (6) (2000) 974–979.
[13] T. Kadota, H. Hiroyasu, Evaporation of a single droplet at elevated pressures and temperatures, Bull. JSME 19 (138) (1976) 1515–1521.
[14] A.T. Shih, C.M. Megaridis, Suspended droplet evaporation modeling in a laminar convective environment, Combust. Flame 102 (1995) 256–270.
[15] J.-R. Yang, S.-C. Wong, On the discrepancies between theoretical and experimental results for microgravity droplet evaporation, Int. J. Heat Mass Transfer 44 (2001) 4433–4443.
[16] K.C. Hsieh, J.S. Shuen, V. Yang, Droplet vaporization in high-pressure environments I: near critical conditions, Combust. Sci. Tech. 76 (1991) 111–132.
[17] H. Jia, G. Gogos, High pressure droplet vaporization: effects of liquid-phase gas solubility, Int. J. Heat Mass Transfer 36 (18) (1993) 4419–4431.
[18] J.-J. Whang, C.-Y. Yukao, J.-T. Ho, S.-C. Wong, Experimental study of the ignition of single droplets under forced convection, Combust. Flame 110 (1997) 366–376.
[19] R.J. Haywood, R. Nafziger, M. Renksizbulut, A detailed examination of gas and liquid phase transient processes in convective droplet evaporation, J. Heat Transfer, Trans. ASME 111 (1989) 495–502.
[20] F.P. Incropera, D.P. DeWitt, in: Fundamentals of Heat and Mass Transfer, fourth ed., John Wiley and Sons, New York, 1996, p. 515.
[21] B. Abramzon, W.A. Sirignano, Droplet vaporization model for spray combustion calculations, Int. J. Heat. Mass Transfer 32 (19) (1989) 1605–1618.

[22] S.W. Churchill, M. Bernstein, Correlating equation for forced convection from gases and liquids to a circular cylinder in crossflow, J. Heat Transfer, Trans. ASME 94 (1977) 300–306.
[23] S.W. Churchill, H.H.S. Chu, Correlation equations for laminar and turbulent free convection from a horizontal cylinder, Int. J. Heat .Mass Transfer 18 (1975) 1049–1053.
[24] C.W. Robert, J.A. Melvin, CRC Handbook of Chemistry and Physics, 61st ed., CRC Press, Boca Raton, FL, 1981, p. F-80.
[25] T.E. Daubert, R.T. Danner, Physical and Thermodynamic Properties of Pure Chemicals, Data Compilation, Hemisphere, New York, 1989.
[26] C.R. Reid, J.M. Prausnitz, B.E. Poling, The Properties of Gases and Liquids, fourth ed., McGraw-Hill, New York, 1987.
[27] M. Nehse, J. Warnatz, C. Chevalier, Kinetic modeling of the oxidation of large aliphatic hydrocarbons, Proceedings of 26th International Symposium on Combustion, The Combustion Institute, Pittsburgh, PA, 1996, 773–780.